Clinical Cancer Research

An Effective Epigenetic-PARP Inhibitor Combination Therapy for Breast and Ovarian Cancers Independent of BRCA Mutations

Nicholas Pulliam[1,2], Fang Fang[2], Ali R. Ozes[1,2], Jessica Tang[2], Adeoluwa Adewuyi[3], Harold Keer[4], John Lyons[5], Stephen B. Baylin[6], Daniela Matei[7], Harikrishna Nakshatri[8], Feyruz V. Rassool[3], Kathy D. Miller[9], and Kenneth P. Nephew[1,2,10,11]

Abstract

Purpose: PARP inhibitors (PARPi) are primarily effective against BRCA1/2-mutated breast and ovarian cancers, but resistance due to reversion of mutated BRCA1/2 and other mechanisms is common. Based on previous reports demonstrating a functional role for DNMT1 in DNA repair and our previous studies demonstrating an ability of DNA methyltransferase inhibitor (DNMTi) to resensitize tumors to primary therapies, we hypothesized that combining a DNMTi with PARPi would sensitize PARPi-resistant breast and ovarian cancers to PARPi therapy, independent of BRCA status.

Experimental Design: Breast and ovarian cancer cell lines (BRCA-wild-type/mutant) were treated with PARPi talazoparib and DNMTi guadecitabine. Effects on cell survival, ROS accumulation, and cAMP levels were examined. *In vivo*, mice bearing either BRCA-proficient breast or ovarian cancer cells were treated with talazoparib and guadecitabine, alone or in combination. Tumor progression, gene expression, and overall survival were analyzed.

Results: Combination of guadecitabine and talazoparib synergized to enhance PARPi efficacy, irrespective of BRCA mutation status. Coadministration of guadecitabine with talazoparib increased accumulation of ROS, promoted PARP activation, and further sensitized, in a cAMP/PKA-dependent manner, breast and ovarian cancer cells to PARPi. In addition, DNMTi enhanced PARP "trapping" by talazoparib. Guadecitabine plus talazoparib decreased xenograft tumor growth and increased overall survival in BRCA-proficient high-grade serous ovarian and triple-negative breast cancer models.

Conclusions: The novel combination of the next-generation DNMTi guadecitabine and the first-in-class PARPi talazoparib inhibited breast and ovarian cancers harboring either wild-type– or mutant-BRCA, supporting further clinical exploration of this drug combination in PARPi-resistant cancers. *Clin Cancer Res; 24(13); 3163–75. ©2018 AACR.*

Introduction

PARP1 is a ubiquitous nuclear enzyme (1) that responds to DNA damage by poly-ADP-ribosylating (PARylating) target proteins including PARP1 itself. PARylation permits PARP1 engagement of the damaged DNA site to stabilize DNA repair complexes (2). A critical role for PARP1 in tumor progression through regulation of intracellular ROS- and oxidation-induced DNA damage has been demonstrated, enhancing both cancer proliferation and chemoresistance (2, 3). PARP1 has also been demonstrated to crosstalk with and compensate for proteins involved in double-strand break (DSB) repair including known tumor suppressors BRCA1 and BRCA2 (4). Dependence on PARP1 for DSB repair in epithelial ovarian cancer and breast cancer harboring mutated BRCA genes has been demonstrated, resulting in exquisite sensitivity to inhibitors of PARP enzymatic activity due to synthetic lethality (5).

PARP inhibitors (PARPi) for treating breast cancer and ovarian cancer have recently been approved by the FDA. Olaparib (Lynparza; olaparib tablets) was approved to treat patients with metastatic breast cancer who have a "BRCA" gene mutation. Lynparza and rucaparib (Rubraca) were approved to treat ovarian cancer patients with mutated BRCA1/2 who received three or more chemotherapy treatments or as maintenance treatment regardless of BRCA status (6, 7). Most recently, niraparib (Zejula) was also approved for maintenance treatment of women with recurrent ovarian cancer who experienced a complete or partial response to platinum-based chemotherapy, independent of BRCA status. However, initially, responsive breast cancer and ovarian cancer eventually develop PARPi resistance due to

[1]Molecular and Cellular Biochemistry Department, Indiana University, Bloomington, Indiana. [2]Medical Sciences Program, Indiana University School of Medicine, Bloomington, Indiana. [3]Department of Radiation Oncology, School of Medicine, University of Maryland, Baltimore, Maryland. [4]Astex Pharmaceuticals, Inc., Pleasanton, California. [5]Astex Therapeutics Limited, Cambridge, United Kingdom. [6]Department of Oncology, Johns Hopkins School of Medicine, Baltimore, Maryland. [7]Department of Obstetrics and Gynecology, Northwestern University Feinberg School of Medicine, Chicago, Illinois. [8]Department of Surgery, Indiana University School of Medicine, Indianapolis, Indiana. [9]Department of Medicine, Indiana University School of Medicine, Indianapolis, Indiana. [10]Department of Cellular and Integrative Physiology, Indiana University School of Medicine, Indianapolis, Indiana. [11]Department of Obstetrics and Gynecology, Indiana University School of Medicine, Indianapolis, Indiana.

Note: Supplementary data for this article are available at Clinical Cancer Research Online (http://clincancerres.aacrjournals.org/).

Prior presentation: This study was presented in part at the 2014 and 2017 meetings of the American Association for Cancer Research.

Corresponding Author: Kenneth P. Nephew, Indiana University School of Medicine, Jordan Hall 302, 1001 E. Third Street, Bloomington, IN 47405-4401. Phone: 812-855-9445; Fax: 812-855-4436; E-mail: knephew@indiana.edu

doi: 10.1158/1078-0432.CCR-18-0204

Translational Relevance

PARP inhibitors (PARPi) are currently FDA approved for BRCA-mutated high-grade ovarian (platinum-responsive) and metastatic breast cancer, as well as for maintenance therapy in ovarian cancer independent of BRCA status. Intrinsic resistance to PARPi therapy due to reversion of mutated BRCA genes and other mechanisms is common, and a therapeutic strategy to sensitize ovarian and breast cancers to PARPi regardless of BRCA mutation status is needed. In preclinical models, we show combining the DNA methyltransferase inhibitor (DNMTi) guadecitabine and the PARPi talazoparib increases ROS accumulation, cAMP/PKA signaling, and subsequent PARP activation. We demonstrate DNMTi–PARPi combinatorial efficacy is also due to chromatin trapping of the respective enzymes by their inhibitors. Coadministration of guadecitabine with talazoparib decreases tumor burden and increases overall survival in ovarian and breast cancer xenograft models. Importantly, the enhanced PARPi response is irrespective of BRCA status. These data suggest further clinical exploration of this drug combination in PARPi-resistant cancers.

reversion of mutated BRCA genes (8) and other mechanisms (9–11), and this class of drug has proven to be ineffective in women with intrinsic or acquired chemoresistance (8, 9). Furthermore, as the vast majority of breast and ovarian tumors are BRCA-proficient, additional approaches for improving PARPi efficacy in these diseases are necessary.

DNA methyltransferase 1 (DNMT1) belongs to a family of enzymes responsible for maintaining cellular DNA methylation patterns in the context of CpG dinucleotides (12). Aberrant DNMT1 activity has been associated with DNA hypermethylation, tumor suppressor gene silencing, and chemoresistance in ovarian and other cancer types (13, 14). Mechanistically, DNMT inhibitors (DNMTi), such as 5-azacytidine (Vidaza) and 5-aza-2′-deoxycytidine (decitabine and guadecitabine), are cytosine analogues that require incorporation into replicating DNA to promote DNA hypomethylation, through formation of DNMT–DNA adducts, and subsequent DNMT degradation (15). Besides epigenetic regulation, upon activation by deoxycytidine kinase, DNMTis increased intracellular ROS accumulation, and subsequent PARP activation was required for DNA repair (16, 17). In addition, preclinical studies have demonstrated increased efficacy of DNMTis when combined with other cancer therapies (reviewed in ref. 14), and recent clinical trials showed DNMTi resensitized platinum-resistant ovarian cancer to carboplatin resulting in patient benefit (18, 19).

Based on previous reports demonstrating a functional role for DNMT1 in DNA repair (DDR; refs. 20, 21) and our previous studies demonstrating DNMTis ability to resensitize tumors to primary therapies (22, 23), we hypothesized that combining a DNMTi with PARPi would sensitize PARPi-resistant ovarian cancer to PARPi therapy, regardless of BRCA status. In support of our hypothesis, it was recently demonstrated that DNMTi–PARPi combination induced PARPi sensitization in leukemia and breast cancer models (24), further suggesting that such a combination approach would impair BRCA-mediated DDR, resulting in cytotoxicity in cells harboring intact or mutant BRCA1/2. Here, we show that combination treatment with the next-generation DNMTi guadecitabine and the first-in-class PARPi talazoparib enhanced PARPi response in both breast and high-grade ovarian cancer cell lines harboring either wild–type– or mutant-BRCA. In addition to enzyme trapping, previously shown (24), we now demonstrate ROS accumulation and modulation of the ROS-cAMP/PKA signaling axis by guadecitabine as a major mechanism underlying response to talazoparib, resulting in increased sensitivity to PARPi therapy irrespective of BRCA status.

Materials and Methods

Cell lines, culture conditions, and reagents

Breast and epithelial ovarian cancer cell lines (see Supplementary Materials and Methods) were maintained in either RPMI-1640 (Invitrogen) as previously described (25) or DMEM (Invitrogen). MCF7 and anti–estrogen-resistant derivatives (MCF7-T, MCF7-F, and MCF7-TF) were maintained and established as we have previously described (26). Triple-negative breast cancer (TNBC) cell line MDA-MB-231 and the metastatic TMD-231 sublines were maintained in RPMI-1640. TMD-231 cells were derived as we have described (27). Cell lines were authenticated in 2012 by the ATCC and tested for mycoplasma contamination. To ensure cell line integrity, cells were not used beyond 30 to 40 passages. Cell culture reagents further described in Supplementary Materials and Methods.

Clonogenic survival and MTT assay

Cells were seeded to 60% to 70% confluency in 10 cm plates and treated for indicated times. Twenty-four hours following treatment, cells were washed, serially diluted, and plated in triplicate on 6-well plates (500–1,000 cells/well). Six to 14 days of cell growth were allowed for colony formation, followed by staining with 0.5% crystal violet. Cell count was normalized to untreated control as previously described (22). See Supplementary Materials and Methods for details regarding drugs and treatment schemas.

RNA extraction, quantitative RT-PCR, and cell transfection

RNA was extracted, cDNA prepared, and qRT-PCR performed as we have previously described (22), using EEF1A as the internal control. Plasmids expressing Maltose Binding Protein (MBP)–tagged BRCA2 and KD BRCA2 constructs have been previously described (28, 29). Overexpression and knockdown vectors (250 ng) were transfected with Turbofect reagent (Thermo scientific) as previously described (25).

cAMP, ROS, ATP, and caspase 3/7 assays

Confluent 10 cm plates were treated as indicated in the text. Following treatment, 2×10^4 cells were plated on 96-well plates. Twenty-four hours after plating cells, cAMP, ATP, caspase 3/7, and ROS (Promega) assays were performed as previously described (25).

Western blot analysis

Total cell lysate was prepared with RIPA lysis buffer, and Western blot analysis was performed as we have previously described (22). Western blot for BRCA2 was performed as

described by Jensen and colleagues (28). Antibodies were as described in Supplementary Materials and Methods.

PARP trapping assay

Chromatin extraction was performed according to Muvarak and colleagues (24), and PARP binding in the chromatin fraction (indicative of PARP trapping) was assayed by Western blot analysis of the chromatin cell fraction against the indicated antibodies, as described (22). Blots were then analyzed by densitometry using ImageJ software (National Institute of Health, Bethesda, MD).

PAR-capture ELISA

Cells were seeded in 10 cm plates, treated as described in the text, harvested, 20% SDS was added (final concentration of 1%), and protein concentration was measured. The lysate was snap-frozen and placed at −80°C. Precoated 96-well plates were incubated with 100 μL of sample (20 μg protein), and PAR concentration was determined according to the manufacturer's protocol (Trevigen; 4520-096-K). The data are reported as the relative change in PAR concentration compared with control.

RAD51 foci formation assay

PEO1 cells transfected with vector or BRCA2 expression plasmid were plated on glass slides (50,000 cells/well), fixed, and permeabilized as described by Sakai and colleagues (31). Antibody concentration and duration are given in Supplementary Materials and Methods. Results are representative of three independent experiments ± SEM.

Combination index and synergism

Cells were treated and plated as indicated for clonogenic survival assays. Following treatment, the percent survival subtracted from 100% was indicative of the fraction affected (FA). Subsequent combination indices, and synergism determination, were determined by the Chou–Talalay method (30; mutually nonexclusive assumption) using CompuSyn Software.

Mouse xenograft experiments

Subcutaneous tumor models. All animal studies adhered to ethical regulations and protocols approved by the Institutional Animal Care and Use Committee of Indiana University. Either OVCAR4 or MDA-MB-231 cells (2×10^6 cells) were s.c. injected into the left flank of 5- to 6-week-old female, athymic nude mice (Harlan). Tumor measurement and drug treatments are described in Supplementary Materials and Methods.

Orthotopic tumor model. TMD-231 cells were injected into the mammary fat pad (*mfp*) of the mice ($n = 28$ total) and allowed to form palpable tumors ($v = 10$ mm^3). Mice were then randomized ($n = 7$ per group), treated, and monitored as described in the Supplementary Materials and Methods.

Statistical analysis

All data, unless noted otherwise, are represented as mean value ± SEM of at least three biological replicates. IC_{50} data were determined by Prism 6 (GraphPad Software), using logarithm-normalized sigmoidal dose-curve fitting. The Tukey test for multiple comparisons correction was used to analyze the significance among different groups in biological assays, unless otherwise stated. For *in vivo* experiments, ANOVA/Mann–Whitney tests (GraphPad) were used to determine statistical significance, as described (23).

Results

BRCA-deficient and -proficient ovarian and breast cancer cells are inhibited by guadecitabine–talazoparib combination

To initially examine the effect of combining a DNMTi with a PARPi on cell growth, the high-grade serous ovarian cancer cell line pair PEO1 and PEO4 (8, 31) was utilized. PEO4 cells were derived from PEO1 cells at the time of acquired chemoresistance, with a noted BRCA2 reversion (30). Differential BRCA2 expression was confirmed between the paired cell lines (Fig. 1A). To restore BRCA2 function in PEO1 cells, we overexpressed BRCA2 (Fig. 1B). Functionality of overexpressed BRCA2 protein in PEO1 cells was validated by increased (~2.7-fold, $P < 0.05$) RAD51 foci, as BRCA2 is required for RAD51 focus formation (Supplementary Fig. S1A; ref. 31), and by MTT cell viability assay (increased cisplatin IC_{50}; Supplementary Fig. S1B; ref. 32). Interestingly, in both PEO4 compared with PEO1 cells and PEO1 cells overexpressing BRCA2 compared with vector control, we observed greater DNMT1 expression (Fig. 1A and B). Furthermore, treatment of PEO1 and PEO4 cells with Talaz increased ($P < 0.05$) DNMT1 expression in both cell lines, regardless of BRCA status (Supplementary Fig. S1C and S1D). These data indicate that DNMT1 may represent a target to overcome PARPi resistance in BRCA2-deficient and -proficient cancer cells.

To investigate whether DNMT1 inhibition altered cell sensitivity to PARPi, PEO1 and PEO4 cells were treated with Talaz alone or in combination with Guad, and colony formation assays were performed. As expected, low-dose (1 nmol/L) Talaz decreased ($P < 0.05$) PEO1 survival but had no effect on clonogenicity of PEO4 cells (Fig. 1C). Despite the differential response to Talaz, coadministration of Guad and Talaz synergistically (CI < 1) decreased ($P < 0.05$; Fig. 2D) cell survival in both PEO1 and PEO4 cells (Fig. 1C; ref. 30). In addition, we observed that Guad treatment alone decreased DNMT1 levels (Fig. 1E) and increased PARP activation, indicated by increased PAR ($P < 0.05$; Fig. 1F). PARP levels following treatment with Talaz alone remained unchanged; however, PARP activity (PARylation) decreased ($P < 0.05$; Fig. 1E and F), in agreement with previous reports (33).

To validate the observed decrease in colony formation was not a cytostatic response, we measured activity and cleavage of caspase 3 by luciferase assay and Western blot analysis, respectively. Combination of DNMTi and Talaz increased both cleaved caspase 3 levels and activity (Fig. 1E; Supplementary Fig. S1E) and Annexin V staining (Supplementary Fig. S1F), indicating that DNMTi–Talaz combination was cytotoxic.

To confirm the combinatorial efficacy of DNMTi–Talaz was not limited to PEO cell lines, we performed clonogenic survival assays in a panel of breast and ovarian cancer cell lines representing BRCA-mutant and wild-type (Supplementary Table S1). Overall response to Talaz alone differed regardless of BRCA status (Supplementary Figs. S2 and S3), consistent with both preclinical and clinical observations with regard to PARPi (34, 35); however, in all cell lines examined, coadministration of DNMTi increased response to Talaz, resulting in a synergistic (CI < 1) decrease ($P < 0.05$) in cell survival, irrespective of BRCA

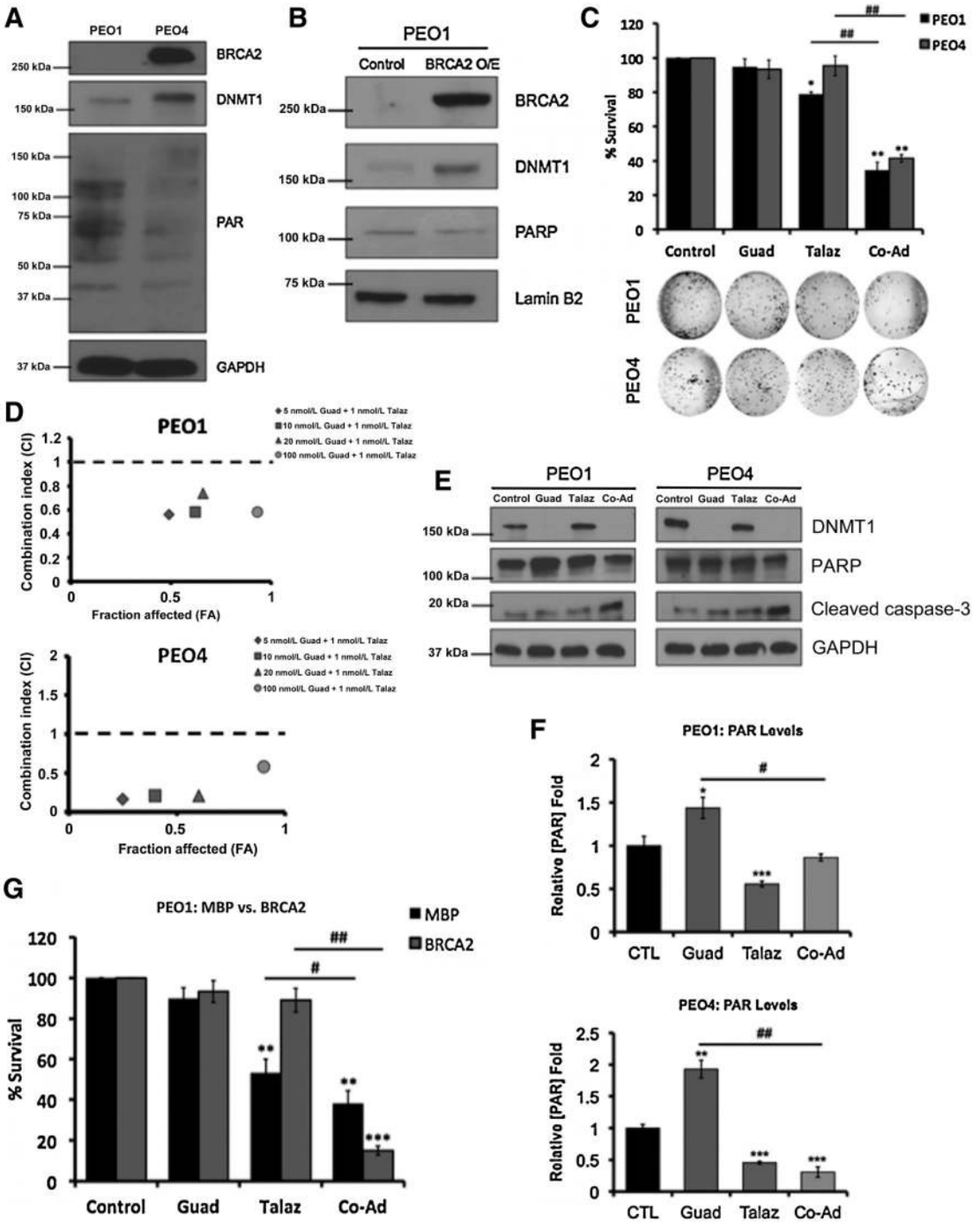

Figure 1.

Therapeutic inhibition of DNMT1 promotes sensitivity to PARPi, independent of BRCA status. Western blot showing endogenous BRCA2 and DNMT1 expression in (**A**) PEO1 and PEO4 cell lines and (**B**) in PEO1 cells overexpressing (O/E) vector control or BRCA2. **C,** PEO1 and PEO4 cells were treated with 20 nmol/L guadecitabine (Guad) or 1 nmol/L talazoparib (Talaz), alone and in combination for 72 hours, and clonogenic cell survival assay was performed. Representative images of formed colonies are below. Quantification is representative of at least three individual experiments. **D,** PEO1 and PEO4 cells were treated with guadecitabine and talazoparib for 72 hours, alone and in combination, and subjected to clonogenic survival assay to determine drug efficacy; *x*-axis is indicative of FA, *y*-axis is indicative of the combination index Combinations beneath the black dashed line are synergistic. PEO1 and PEO4 cells were treated with 20 nmol/L Guad or 1 nmol/L Talaz for 72 hours, alone and in combination. **E,** Cell lysates were subjected to Western blot analysis against the indicated antibodies or (**F**) PAR-capture ELISA to measure PAR levels. **G,** PEO1 cells ectopically expressing BRCA2 or vector control were treated with 20 nmol/L Guad and 1 nmol/L Talaz, alone or in combination, and subjected to colony formation assays. Results are representative of three independent experiments (mean ± SEM). *, $P < 0.01$; **, $P < 0.001$; ***, $P < 0.0001$ compared with control; #, $P < 0.01$ and ##, $P < 0.001$ relative to bracketed treatment.

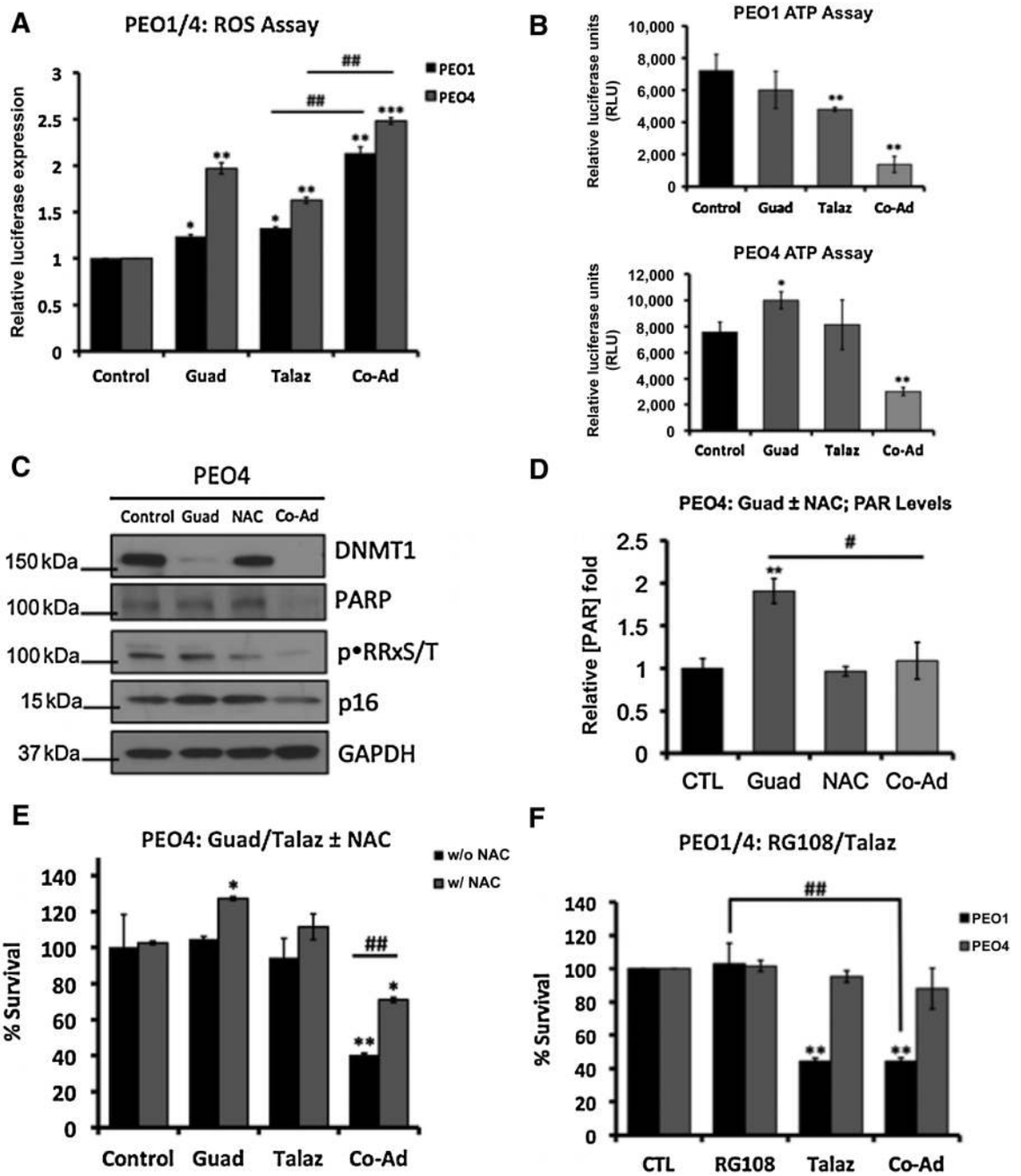

Figure 2.

Guadecitabine mediates PARP activation through increased intracellular ROS accumulation. **A,** PEO1 and PEO4 cells were treated with either 20 nmol/L guadecitabine (Guad) or 1 nmol/L talazoparib (Talaz) for 72 hours, alone and in combination. Twenty-four hours after treatment, intracellular ROS was measured. Quantification is representative of three individual experiments. **B,** PEO1 (top) and PEO4 (bottom) cells were treated for 72 hours with 20 nmol/L Guad or 1 nmol/L Talaz, alone and in combination, and 24 hours after treatment, ATP was measured. Quantification is representative of three individual experiments. PEO4 cells were treated with 20 nmol/L Guad, with and without 1 mmol/L NAC (ROS-scavenger) before treatment (1 hour). **C,** Cell lysates were subjected to Western blot analysis against the indicated antibodies or (**D**) PAR-capture ELISA to measure PAR levels. **E,** PEO4 cells were treated with 20 nmol/L Guad or 1 nmol/L Talaz, alone and in combination, for 72 hours, with or without 1 mmol/L NAC and subjected to colony formation assays. Quantification is representative of three independent experiments. **F,** PEO1 and PEO4 cells were treated with 5 μmol/L RG108 (nonnucleoside analogue) or 1 nmol/L Talaz alone and in combination for 72 hours, and subjected to colony formation assays. Results are representative of three independent experiments. *, $P < 0.05$; **, $P < 0.001$; and ***, $P < 0.0001$ compared with control; #, $P < 0.01$ and ##, $P < 0.001$ relative to bracketed treatment.

status (Supplementary Figs. S2 and S3). Similarly, sequential treatment ("prime") of Guad prior to Talaz increased ($P < 0.05$) cell death in the majority of ovarian cancer cells (Supplementary Fig. S2), although often not to the extent of DNMTi–PARPi coadministration. Interestingly, with respect to the breast cancer cell lines, we observed overall Guad–Talaz "priming" resulted in similar cell death compared with Guad alone (Supplementary Fig. S3).

In addition to intrinsic resistance, reversion of mutated BRCA1/2 is a widely reported mechanism of therapy-induced resistance to PARPi (8–10). To further examine the role of BRCA2 in DNMTi-mediated sensitivity to PARPi, we either knocked down BRCA2 in PEO4 cells or overexpressed BRCA2 in both PEO1 and PEO4 cells and performed clonogenic survival assays. BRCA2 knockdown sensitized PEO4 cells to Talaz, and cells remained sensitive to combination of Guad and Talaz (Supplementary Fig. S4A and S4B). Overexpressing BRCA2 in PEO4 cells did not rescue Guad-mediated sensitization to Talaz (Supplementary Fig. S4C and S4D). As expected, PEO1 cells ectopically expressing BRCA2 (Fig. 1B) were resistant to Talaz treatment (Fig. 1F); however, in response to combination of Guad and Talaz, cell survival decreased ($P < 0.05$; Fig. 1G). Collectively, these results are consistent with our previous observations demonstrating DNMT1 as a target to overcome therapeutic resistance (26, 36) and further indicate that DNMTi increases response to PARPi, regardless of BRCA-mediated DDR.

Guadecitabine-mediated PARP activation through increased intracellular ROS

Because overexpression of BRCA2 was not able to reverse the effects of Guad–Talaz coadministration, we investigated the mechanism of Guad-mediated PARPi sensitivity. Interestingly, Guad increased PAR levels in both PEO1 and PEO4 cells (Fig. 1F). In a leukemia model, it was recently demonstrated that nucleoside-based DNMTi, prior to obligate incorporation into DNA, increased ROS (17), resulting in DNA damage and PARP activation, which, if unresolved, promoted cell death (37). Based on these reports, we investigated whether Guad increased ROS and if increased ROS was responsible for PARP activation and PARPi response. PEO1 and PEO4 cells were treated with Guad in the presence and absence of Talaz, and intracellular ROS levels were measured. Guad alone increased ($P < 0.05$) ROS levels in both PEO1 and PEO4 cells, and Guad–Talaz coadministration further increased ($P < 0.05$) ROS levels (Fig. 2A). Interestingly, in PEO4 cells, we observed a greater increase in ROS in response to Guad alone, compared with PEO1, consistent with decreased PARP activity in PEO4 cells (Supplementary Fig. S5A).

Tight regulation of intracellular ROS is integral for cell survival and cancer progression (38). Positive bioenergetic coupling between ROS generation and ATP levels was demonstrated, and conversely, ROS accumulation sufficient to promote cell death induced ATP depletion (39). To investigate the relationship between Guad-mediated ROS accumulation and PARPi sensitivity, we measured ATP levels following Guad treatment with or without Talaz. Consistent with Guad-induced ROS accumulation in PEO4 cells, we observed increased ($P < 0.05$) ATP levels in response to Guad treatment (Fig. 2B; Supplementary Fig. S5B). Moreover, Guad–Talaz coadministration depleted ($P < 0.05$) ATP levels in both PEO1 and PEO4 cells, indicating increased PARPi response. Furthermore, in Talaz-treated PEO4 cells, decreased (~20%, $P < 0.05$) expression of genes whose enzymes products produce ROS was observed (Supplementary Fig. S5C–S5E), in support of a role of ROS-associated genes in chemoresistance (38, 40). Consistent with this observation, no change in expression of ROS-associated genes was observed in Talaz-treated PEO1 cells (Supplementary Fig. S5D). However, in both PEO1 and PEO4 cells, Guad–Talaz coadministration increased ($P < 0.05$) ROS-associated gene expression (Supplementary Fig. S5D and S5E), correlating increased PARPi sensitivity with ROS modulation (38).

Given that Guad treatment increased intracellular ROS, which subsequently increased PARP activity, we hypothesized that Guad-dependent ROS accumulation contributed to PARP activation and subsequent PARPi sensitivity. To test this, we treated PEO4 cells with Guad, in the presence and absence of the ROS-scavenger N-acetyl-L-cysteine (NAC). We observed that combination of Guad and NAC decreased both PARP and PAR levels, as well as known ROS-responsive proteins p16 and PKA (41, 42), indicated by decreased phosphorylation of the PKA substrate motif (pRRXS/T), compared with Guad alone (Fig. 2C and D, respectively).

Next, to investigate whether increased ROS and subsequent PARP activation mediated by Guad (demonstrated above) promoted PARPi sensitivity (38), PEO4 cells were treated with Guad and Talaz with or without NAC and subjected to clonogenic survival. As previously demonstrated (Fig. 1C), combination of Guad and Talaz induced cytotoxicity, whereas the addition of low dose (1 mmol/L) NAC significantly ($P < 0.05$) rescued the induced cell death (Fig. 2E). We then inhibited DNMT1 using a nonnucleoside DNMTi RG108 (Supplementary Fig. S5F). Previous reports demonstrated "direct" DNMTi, which do not incorporate into DNA (such as RG108), had no effect on ROS accumulation (17). Consistent with these reports, no increase in ROS was observed after RG108 treatment (Supplementary Fig. S5G). We then treated PEO1 and PEO4 cells with RG108, with and without Talaz, and performed clonogenic survival assays. As expected, Talaz alone decreased ($P < 0.05$) cell survival in PEO1, but not PEO4 cells (Fig. 2F), and coadministration with RG108 had no effect on Talaz response in either cell line. Collectively, these results suggest that Guad increases PARPi sensitivity in a ROS-dependent manner, representing a potential approach to overcome PARPi resistance.

Guadecitabine-induced ROS increased activation of cAMP/PKA signaling and PARP

ROS was demonstrated to activate cellular kinases to promote PARP activation (16). As such, we investigated the underlying mechanism regulating PARP activation in response to Guad-mediated ROS accumulation. We previously observed that combination of Guad and NAC diminished not only PAR levels but also PKA activity (decreased pRRXS/T; Fig. 2C). It was recently demonstrated that PKA activation, under oxidative stress conditions and in response to the second messenger cAMP, induced rapid PARP activation and DNA repair (41). To investigate ROS ability to activate PARP in a PKA-dependent manner, PEO4 cells were treated with H_2O_2 (1 mmol/L) in the presence and absence of PKA inhibitor H89 (5 μmol/L) and subjected to Western blot analysis. In response to H_2O_2, increased PARP and PKA activation (increased pCREB) was observed, as demonstrated with Guad, and subsequent

inhibition of PKA was sufficient to reduce PARP activity (Supplementary Fig. S6A), consistent with previous reports (16, 41). To further validate PKA-mediated PARP activation, we ectopically expressed either vector control or PKA (Fig. 3A, left). Overexpression of PKA increased PAR levels compared with vector control, and successive treatment with Talaz decreased PARP activity in both vector- and PKA-overexpressing cells (Fig. 3A, right).

It was next of interest to determine whether PKA-mediated PARP activation affected PARPi response. We treated PEO4 cells overexpressing either vector control or PKA with or without Talaz and performed clonogenic survival assays. We observed that PEO4 cells overexpressing vector control remained resistant to Talaz treatment, whereas PKA overexpression was sufficient to promote sensitivity to Talaz (Fig. 3B). To examine whether Guad-mediated PARP activation was PKA-dependent, PEO4 cells were treated with Guad, in the presence and absence of PKA inhibitor H89. Guad increased PARP activation (PARylation), and coadministration with H89 blocked PARP activation (Fig. 3C), indicating that Guad-induced ROS accumulation increased PARP activation in a PKA-dependent manner.

To further investigate the relationship between PKA activation and PARPi response, we measured changes in the second messenger, cAMP, following Talaz treatment, with and without Guad. Talaz decreased (~70%, $P < 0.05$) intracellular cAMP in PARPi-resistant PEO4 cells, but not in the PEO1 cell line (Fig. 3D and E). Guad–Talaz coadministration increased ($P < 0.05$) cAMP levels in both PEO1 and PEO4 cells compared with Talaz treatment alone (Fig. 3D and E), indicative of increased PARPi response. In addition, basal cAMP levels did not differ between the cell lines, despite their differential response to Talaz (Supplementary Fig. S6B), as previously described (43). To extend this observation, cAMP levels following Talaz treatment were examined in a panel of breast and ovarian cancer cell lines differing in sensitivity to PARPi (Supplementary Fig. S6C). Similar to PEO4 cells, Talaz decreased cAMP levels in PARPi-resistant versus -sensitive cell lines (Supplementary Figs. S2 and S3), regardless of BRCA status in most cell lines examined, indicating that cAMP response may represent an additional determinant of PARPi sensitivity.

Because combination of Guad and Talaz increased intracellular cAMP, we investigated whether increased cAMP affected PARP levels, and subsequent sensitivity to PARPi. In both PEO1 and PEO4 cells, treatment with adenylate cyclase activator forskolin (FSK) increased PARP levels, and subsequent treatment with PKA inhibitor H89 decreased PARP (Supplementary Fig. S6D). To examine the effect of increased cAMP levels on PARPi sensitivity, we treated PEO4 cells with FSK in the presence and absence of Talaz and performed colony formation assays. As expected, Talaz alone did not affect cell survival; however, combination of FSK and Talaz decreased ($P < 0.05$) cell survival (Fig. 3F), and treatment with the PKA inhibitor H89 in the presence of FSK–Talaz decreased ($P < 0.05$) cell death compared with FSK–Talaz coadministration (Fig. 3F). Further, overexpression of BRCA2 in PEO4 cells did not prevent FSK–Talaz-induced cell death (Supplementary Fig. S6E), similarly demonstrated for Guad–Talaz coadministration (Supplementary Fig. S4D). Based on these results, we speculated that inhibition of PKA in the presence of combination of Guad and Talaz would reverse Guad-mediated PARPi response. To test this, we treated PEO4 cells with Guad and increasing concentrations of Talaz, with or without H89, and performed clonogenic survival assays. In the absence of PKA inhibitor, a dose-dependent decrease ($P < 0.05$) in cell survival was observed in response to Guad–Talaz coadministration, and the addition of H89 prevented Guad-mediated sensitization to PARPi (Fig. 3G). Interestingly, a similar reversal of PARPi sensitivity was observed in PEO1 cells following treatment with Talaz in the presence of H89 (Supplementary Fig. S6F). Together, these results suggest that Guad-mediated ROS accumulation promotes PARP activation in a PKA-dependent manner, priming the cell toward PARPi sensitivity, irrespective of BRCA status.

Coadministration of guadecitabine and talazoparib is effective in an ovarian cancer xenograft model

Due to the clinical impact of PARPis in ovarian cancer, and subsequent resistance, we investigated whether addition of Guad could promote PARPi response *in vivo*. BRCA-proficient OVCAR4 cells were subcutaneously injected into mice and allowed to form tumors. Following tumor formation, mice were treated with either vehicle (CTL), single-agent Guad (0.5 mg/kg) and Talaz (0.25 mg/kg), or the combination (Co-Ad), and tumor volume measured at indicated time points (Fig. 4A). Interestingly, in this BRCA-proficient model, treatment with Talaz alone modestly decreased (day 35 onward) overall tumor volume compared with CTL, and Guad alone decreased ($P < 0.05$, day 38 forward) tumor burden compared with the CTL group. Moreover, coadministration of Guad and Talaz further decreased ($P < 0.05$, day 8 onward) tumor volume compared with CTL, Guad, and Talaz treatments alone. Consistent with the observed decrease in tumor volume, we observed single-agent Guad and Talaz decreased ($P < 0.05$) final tumor weight compared with CTL, and coadministration of Guad and Talaz further decreased ($P < 0.05$) final tumor weight compared with all conditions (Fig. 4B). Importantly, drug doses were well tolerated, indicated by increasing body weight gains in each treatment group (Fig. 4C).

The study was ended after 60 days, and RNA was extracted from tumors for qRT-PCR analysis of ROS-associated genes. Treatment with Talaz alone decreased gene expression (Fig. 4D; consistent with our *in vitro* model), and combination of Guad and Talaz increased expression of the ROS-associated genes compared with Talaz alone (Fig. 4D), consistent with gained PARPi sensitivity. H&E staining validated high-grade serous ovarian cancer morphology (Fig. 4E).

Coadministration of guadecitabine and talazoparib is effective in TNBC xenograft models

As resistance to PARPi has also been reported in breast cancer patients (16, 44), we extended our xenograft model to include BRCA-proficient TNBC cell line models MDA-MB-231 and its variant TMD-231. MDA-MB-231 cells (BRCA-proficient) were subcutaneously injected into the flank of mice and allowed to form tumors. Following tumor formation, mice were treated as described for the ovarian cancer xenograft model, and tumor volume was measured. Compared with CTL, treatment with either Talaz (0.25 mg/kg) or Guad (0.5 mg/kg) did not significantly decrease tumor burden (Fig. 5A). However, coadministration of Guad and Talaz decreased ($P < 0.05$, day 8 onward) tumor volume compared with all treatment conditions. In addition to decreased tumor burden, coadministration of Guad and Talaz increased ($P < 0.05$) percent survival

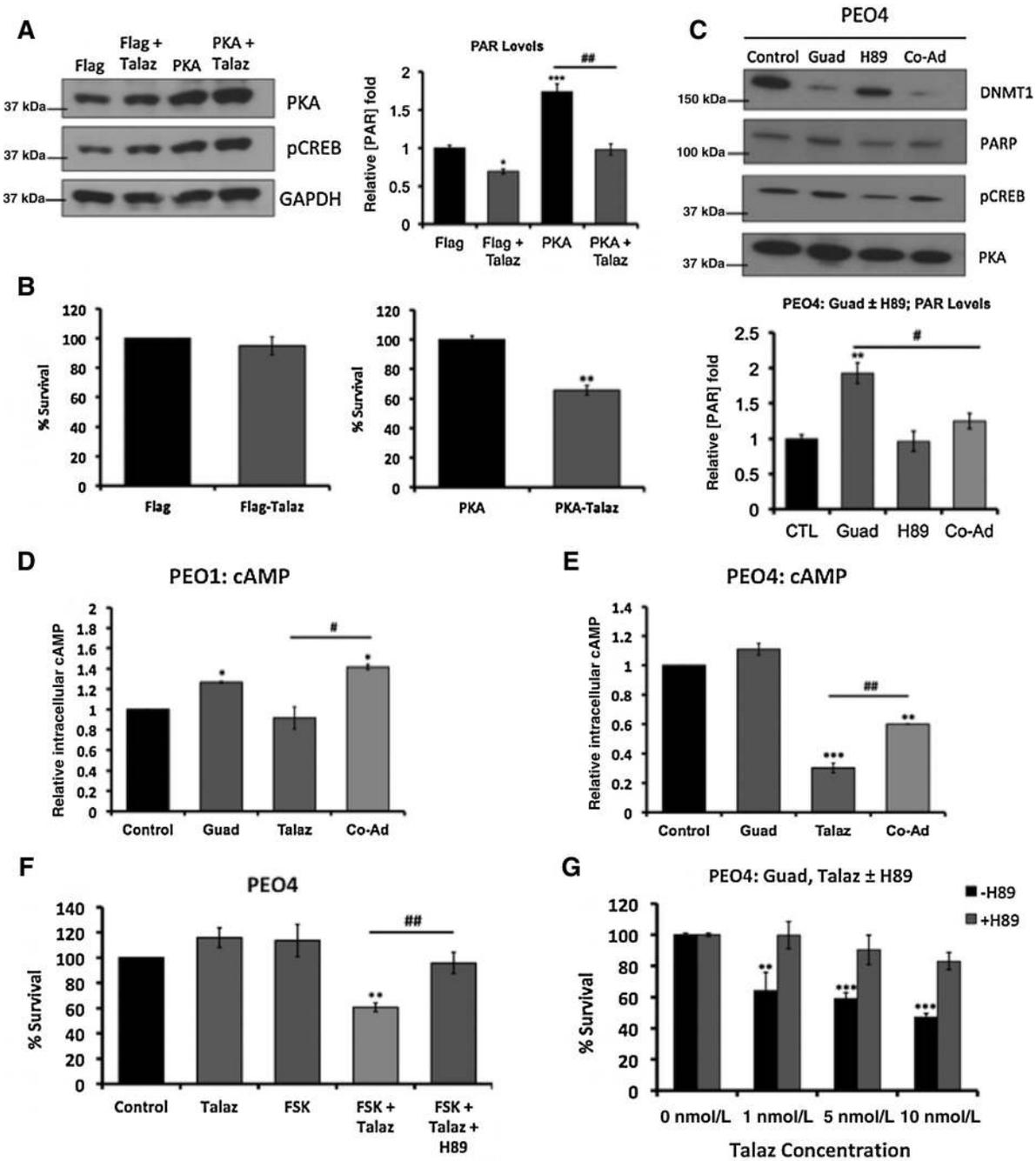

Figure 3.

Guadecitabine-induced ROS accumulation increases cAMP/PKA signaling and PARP activation. **A,** PEO4 cells ectopically expressing PKA or vector control were treated with or without 1 nmol/L talazoparib (Talaz) for 24 hours. Cell lysates were subjected to Western blot analysis against the indicated antibodies and PAR-capture ELISA to measure PAR levels. **B,** Vector control and PKA-overexpressing PEO4 cells were treated with 1 nmol/L Talaz, and clonogenic survival assay was performed. Results are representative of three independent experiments. **C,** PEO4 cells were treated with 20 nmol/L guadecitabine (Guad) with or without 5 μmol/L PKA inhibitor H89 for 72 hours. Twenty-four hours after treatment, cell lysates were subjected to Western blot analysis and PAR-capture ELISA to measure PAR levels. PEO1 (**D**) and (**E**) PEO4 cells were treated with 20 nmol/L Guad or 1 nmol/L Talaz, alone and in combination, for 72 hours. Twenty-four hours after treatment, cAMP levels were measured. Results are representative of three independent experiments. **F,** PEO4 cells were treated with 10 μmol/L FSK or 1 nmol/L Talaz, alone and in combination, in the presence and absence of 5 μmol/L PKA inhibitor H89; clonogenic survival assay was performed. Results are representative of three independent experiments. **G,** PEO4 cells overexpressing vector control or BRCA2 were treated with the indicated concentration of Talaz, in the presence or absence of 10 μmol/L FSK for 48 hours, and subjected to cell viability assays. Results are representative of three independent experiments, performed in duplicate. *, $P < 0.01$; **, $P < 0.001$; and ***, $P < 0.0001$ compared with control; #, $P < 0.01$ and ##, $P < 0.001$ relative to bracketed treatment.

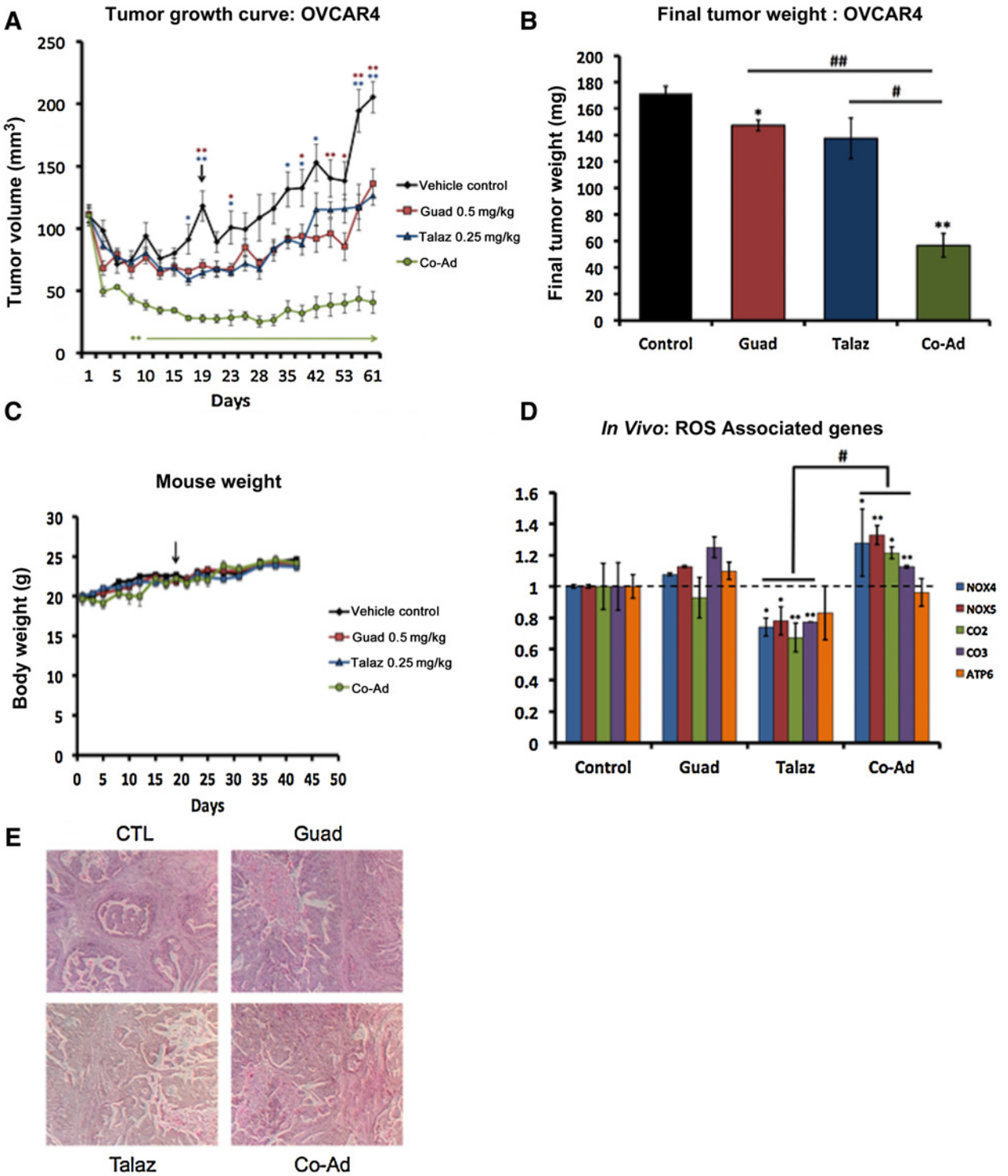

Figure 4.

Coadministration of guadecitabine and talazoparib effective in ovarian cancer xenograft model. **A,** 2×10^6 OVCAR4 cells (high-grade serous ovarian cancer cell line and BRCA1/2 proficient) were subcutaneously injected into the flank of nude mice ($n = 20$) and subsequently randomized ($n = 5$) to treatment groups. When tumors reached 100 mm^3, mice were treated daily (5 times per week) with guadecitabine (Guad; 0.5 mg/kg, s.c.) or talazoparib (Talaz; 0.25 mg/kg, oral gavage) for three cycles. Tumor volume was measured at the indicated time points. Day 0 indicates treatment initiation. Statistically significant difference in tumor volume (until end of the study) is denoted by an asterisk and arrow. **B,** At the end of the study, final tumor weight was measured. **C,** Tumor-bearing mice were weighed at indicated time points throughout the duration of the study. **D,** qRT-PCR analysis ROS-associated genes in excised tumors at the end of the study. **E,** Representative hematoxylin–eosin staining of tumors from each group. *, $P < 0.01$; **, $P < 0.001$; and ***, $P < 0.0001$ compared with control; #, $P < 0.01$ and ##, $P < 0.001$ relative to bracketed treatment.

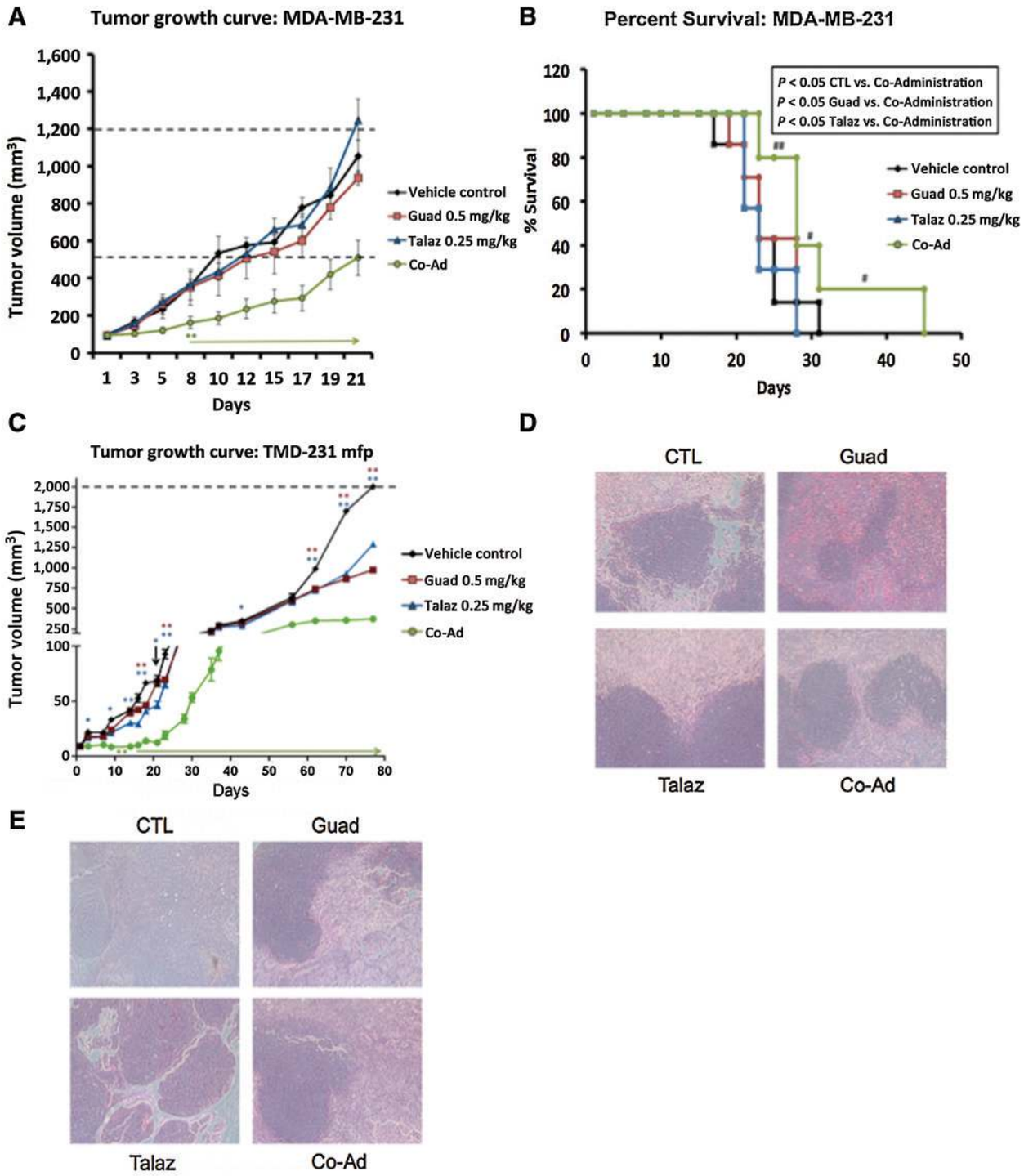

Figure 5.

Coadministration of guadecitabine and talazoparib effective in TNBC xenograft model. **A,** MDA-MB-231 cells (2×10^6) were subcutaneously injected into the flank of nude mice (total $n = 28$) and then randomized to each group ($n = 7$). When tumors reached 100 mm^3, mice were treated daily (5 times per week) with guadecitabine (Guad; 0.5 mg/kg, s.c.) or talazoparib (Talaz; 0.25 mg/kg, orally) for three cycles. Tumor volume was measured at the indicated time points. Day 0 indicates treatment initiation. Statistically significant difference in tumor volume (until end of the study) is denoted by an asterisk and arrow. **B,** Percent survival was measured by sacrifice of mice once tumor volume reached 2,000 mm^3 or showed necrosis. The "#" denotes mice which were removed due to formation of necrosis. **C,** TMD-231 cells (0.5×10^6) were injected into the mammary fat pad (*mfp*) of nude mice (total $n = 28$) and then randomized to each group ($n = 7$). When tumors reached 10 mm^3, mice were treated daily (5 times per week) with Guad (0.5 mg/kg, s.c.) or Talaz (0.25 mg/kg, oral gavage) for three cycles. Tumor volume was measured at the indicated time points. Representative hematoxylin–eosin staining of (**D**) MDA-MB-231 tumors and (**E**) TMD-231 tumors. *, $P < 0.01$; **, $P < 0.001$; and ***, $P < 0.0001$ compared with control.

compared with either single agent and CTL conditions (Fig. 5B). The observed effect in percent survival was in fact dampened due to formation of necrosis and removal of mice on that basis (rather than tumor volume). In this regard, both single agent Guad and Talaz, as well as the combination treatments were well tolerated, as indicated by steady body weight gain under all treatment conditions (data not shown).

We next utilized an orthotopic breast tumor model, considered more clinically relevant and better predictive models of drug efficacy than standard subcutaneous models. TMD-231 cells (derived from MDA-MB-231 cells injected into the mammary fat pad of mice) represent a more aggressive model (27). To reflect the original microenvironment, TMD-231 cells were implanted directly into the mammary fat pad (mfp) of female nude mice. Upon formation of palpable tumors, mice were treated as above with single agent Guad (0.05 mg/kg) and Talaz (0.25 mg/kg) or the combination, and tumor volume was measured at the indicated time points (Fig. 5C). Following treatment with either single agent Guad or Talaz, tumor burden remained unchanged until day 62 compared with the CTL group; however, coadministration of Guad and Talaz inhibited ($P < 0.05$) tumor volume starting on day 14 (Fig. 5C). Subsequently, H&E staining of xenograft tumors was performed to validate breast cancer morphology (Fig. 5D, MBA-MB-231 s.c. tumors; Fig. 5E, TMD-231 mfp tumors).

Discussion

PARPis have demonstrated single-agent efficacy in breast and ovarian cancer as well as other cancer populations with BRCA1/2 deficiencies (35). However, the majority of patients present with BRCA-proficient disease and are not eligible for this important class of drug. Furthermore, most patients develop resistance to PARPi, including through reversion of mutated BRCA1/2 (reviewed in ref. 10). Attempts to overcome PARPi resistance, through both development of more potent PARPi and combination therapies which decrease efficiency of DSB repair (44, 45), have met with limited success, signifying a need to better understand therapeutic options to exploit PARPis clinically independent of BRCA status.

In this study, regardless of BRCA status and without augmentation by platinum-based chemotherapy, we demonstrate that addition of a DNMTi increased cell response to PARPi treatment both *in vitro* and *in vivo*. *In vitro*, combination of DNMTi and Talaz decreased clonogenic survival, cell proliferation (data not shown), and increased caspase 3/7 cleavage. Further, our study revealed that increased PARP activation by Guad was in part ROS-dependent and that PKA was a major regulator of PARP activation and subsequent PARPi response. *In vivo*, we demonstrate that combination of Guad and Talaz decreased tumor burden in both BRCA-proficient ovarian and breast cancer xenograft models and increased overall survival. Importantly, the Guad and Talaz combination was well tolerated in mice. These results are consistent with our previous work demonstrating an ability of DNMTis to resensitize cells to chemotherapy (26, 46).

DNMT1 has been previously implicated in mediating DSB repair through recruitment to sites of DNA damage and epigenetically regulating the damaged site, which we postulated may induce a state of "BRCAness" and therefore PARPi sensitivity (20, 21). Importantly, with respect to our overall hypothesis, we demonstrate that ectopic expression of BRCA2 may modulate response to PARPi but is unable to reverse Guad-mediated PARPi sensitivity, indicating that BRCA-mediated DDR is not the major mechanism of Guad-induced PARPi response. This is further demonstrated through use of the PEO1 and PEO4 cell lines, in which PEO4, derived from PEO1, has a reverting BRCA2 mutation (31). Alternatively, we note that Guad treatment increases PARP activation. Based on these observations, we propose that Guad induces a PARP-mediated DNA damage response, which increases sensitivity to loss of PARP activity, independent of DSB repair (47).

With respect to the above possibilities, besides epigenetic regulation, DNMTis that incorporate into DNA increase intracellular ROS, contributing to their efficacy (17). Of note, increased ROS signaling has been hypothesized as a potential mechanism to overcome PARPi resistance, as well as a unique modality to therapeutically target cancer cells specifically (38). In support of this hypothesis, we demonstrate that Guad treatment alone, or combined with Talaz, increased ROS accumulation in both PEO1 and PEO4 cell lines; moreover, in PEO4 (BRCA-proficient) cells, we observe a greater increase in ROS accumulation following Guad alone, compared with PEO1. ROS scavenging following DNMTi treatment decreased PARP activation and subsequent sensitivity to Guad–Talaz coadministration. Similarly, the nonnucleoside DNMTi RG108, which does not increase intracellular ROS, had no effect on cellular response to Talaz. In support of these findings, in our previous study demonstrating efficacy of combination of DNMTi and PARPi in AML and breast cancer, shRNA-mediated knockdown of DNMT1 was not sufficient to induce PARPi sensitivity (24) and does not affect ROS levels (17). As such, we posit that DNMTi treatment results in PARP activation, and ultimately PARPi response, in a ROS-dependent manner.

In addition to demonstrating DNMTi-mediated PARP activation is in part ROS-dependent, our results link ROS accumulation by Guad to PKA activation. The cAMP/PKA pathway regulates cell fate via multiple mechanisms, including rapid PARP activation, under oxidative stress conditions (41). Previous reports demonstrate, in response to DNA-damaging chemotherapies, a resultant decrease in intracellular cAMP in chemoresistant cells (43). Furthermore, upon reactivation of the pathway, resensitization to therapy was observed (48). Similarly, we demonstrate in cells resistant to PARPi that treatment with Talaz decreases cAMP levels, and both genetic (PKA overexpression) activation and pharmacologic (forskolin) activation of the pathway are sufficient to increase PARPi response. In addition, both ROS depletion and PKA inhibition are sufficient to decrease PKA and PARP activation.

Although our proposed mechanism of DNMTi-mediated PARPi sensitivity focuses on ROS stimulation and PARP activation, we do not believe this to be a mutually exclusive mechanism of induced PARPi response. Combination of DNMTi and Talaz increases PARP localization to chromatin and colocalization with γH2Ax foci in breast cancer and leukemia models, resulting in PARPi sensitivity (24, 49), and in the current study, PARP1 chromatin localization increases in ovarian cancer cells following DNMTi–PARPi coadministration (Supplementary Fig. S7A). Further, DNMT1 localization to DNA is highly specific for ROS-induced DNA damage, and ROS induces DNA methylation (21). Our data support these models and build upon their conclusions. As we show Guad treatment increases

intracellular ROS and promotes PARP activation, we hypothesize that this may in part act as the damage to which DNMT1 and PARP colocalize and are subsequently trapped by their inhibitors, aiding in the PARPi response. This may explain why RG108 was not able to increase cell response to PARPi. In addition, ROS are known to induce several classes of DNA damage, including single-strand breaks and DSBs, as well as base excision repair, to which DNMT1 and PARP may colocalize, potentially amplifying the efficacy of combination of DNMTi and PARPi (49). To further support a ROS—cAMP–PKA-dependent mechanism for PARPi sensitivity, we instead treated PEO1 and PEO4 cells with veliparib (Velip), a much less potent PARP trapper (33, 50), with and without DNMTi, and performed colony formation assays. Even with the less potent PARP trapper, decreased ($P < 0.05$) cell survival was observed after coadministration with Guad. Furthermore, we observed, as with talazoparib, veliparib decreased ($P < 0.05$) cAMP levels in PEO4 cells, not observed in PEO1 (BRCA2-deficient) cells.

In summary, we show addition of DNMTi increases cell response to PARPi, irrespective of BRCA status, both *in vitro* and *in vivo*. In addition to PARP trapping, we put forth a complementary model of Guad-mediated ROS accumulation and subsequent PKA activation (Supplementary Fig. S7B). Activation of the cAMP/PKA system increases PARP activity, "priming" the cell toward PARPi sensitivity, irrespective of BRCA status. Collectively, these results suggest further clinical exploration, as is underway in patients with acute myeloid leukemia (NCT02878785), of DNMTi–PARPi combination for patients with either intrinsic or therapy-induced resistance to PARPi.

Disclosure of Potential Conflicts of Interest

D. Matei is a consultant/advisory board member for Astex and Astra Zenecca. No potential conflicts of interest were disclosed by the other authors.

Authors' Contributions

Conception and design: N. Pulliam, A. Adewuyi, J. Lyons, D. Matei, H. Nakshatri, K.P. Nephew
Development of methodology: N. Pulliam, F. Fang, A.R. Ozes, K.P. Nephew
Acquisition of data (provided animals, acquired and managed patients, provided facilities, etc.): N. Pulliam, J. Tang, K.P. Nephew
Analysis and interpretation of data (e.g., statistical analysis, biostatistics, computational analysis): N. Pulliam, F. Fang, A.R. Ozes, K.D. Miller, K.P. Nephew
Writing, review, and/or revision of the manuscript: N. Pulliam, A.R. Ozes, H. Keer, J. Lyons, S.B. Baylin, D. Matei, F.V. Rassool, K.D. Miller, K.P. Nephew
Administrative, technical, or material support (i.e., reporting or organizing data, constructing databases): H. Keer, J. Lyons, H. Nakshatri, K.P. Nephew
Study supervision: N. Pulliam, D. Matei, K.P. Nephew
Other (contributed to figures in the Supplementary Data): F.V. Rassool

Acknowledgments

We thank Dr. Ryan Jensen (Yale University) for 2X-MBP and 2X-MBP–tagged BRCA2 overexpression constructs, as well as BRCA2 knockdown and control constructs. We thank Sue Childress for preparation of H&E-stained *in vivo* tumor slide preparation. We thank Dr. Susan Perkins (Professor of Biostatistics and Biostatistics Core member at the IS Simon Cancer Center) for assistance with statistical analysis and review of the article. We thank Dr. R. Daniel Lodge-Rigal for initial H&E slide visualization. We thank Pietro Taverna (former: Astex Pharmaceuticals Inc., currently Sunesis Pharmaceuticals) and Len Post (former: BioMarin Pharmaceutical Inc.). This work was supported by NIH R01-CA182832, The V Foundation for Cancer Research Translational Grant (Cary, NC), Indiana Clinical and Translational Sciences Institute TL1 (UL1TR001108; A. Shekhar), and the Adelson Medical Research Foundation.

The costs of publication of this article were defrayed in part by the payment of page charges. This article must therefore be hereby marked *advertisement* in accordance with 18 U.S.C. Section 1734 solely to indicate this fact.

Received January 17, 2018; revised February 23, 2018; accepted March 22, 2018; published first April 3, 2018.

References

1. Kim MY, Zhang T, Kraus WL. Poly(ADP-ribosyl)ation by PARP-1: 'PAR-laying' NAD+ into a nuclear signal. Genes Dev 2005;19:1951–67.
2. Luo X, Kraus WL. On PAR with PARP: cellular stress signaling through poly(ADP-ribose) and PARP-1. Genes Dev 2012;26:417–32.
3. Fruehauf JP, Meyskens FL Jr.Reactive oxygen species: a breath of life or death? Clin Cancer Res 2007;13:789–94.
4. Farmer H, McCabe N, Lord CJ, Tutt AN, Johnson DA, Richardson TB, et al. Targeting the DNA repair defect in BRCA mutant cells as a therapeutic strategy. Nature 2005;434:917–21.
5. Bryant HE, Schultz N, Thomas HD, Parker KM, Flower D, Lopez E, et al. Specific killing of BRCA2-deficient tumours with inhibitors of poly(ADP-ribose) polymerase. Nature 2005;434:913–7.
6. O'Connor MJ. Targeting the DNA damage response in cancer. Mol Cell 2015;60:547–60.
7. Syed YY. Rucaparib: first global approval. Drugs 2017;77:585–92.
8. Barber LJ, Sandhu S, Chen L, Campbell J, Kozarewa I, Fenwick K, et al. Secondary mutations in BRCA2 associated with clinical resistance to a PARP inhibitor. J Pathol 2013;229:422–9.
9. Chiarugi A. A snapshot of chemoresistance to PARP inhibitors. Trends Pharmacol Sci 2012;33:42–8.
10. Lord CJ, Ashworth A. Mechanisms of resistance to therapies targeting BRCA-mutant cancers. Nat Med 2013;19:1381–8.
11. Kondrashova O, Nguyen M, Shield-Artin K, Tinker AV, Teng NNH, Harrell MI, et al. Secondary somatic mutations restoring RAD51C and RAD51D associated with acquired resistance to the PARP inhibitor rucaparib in high-grade ovarian carcinoma. Cancer Discov 2017;7:984–98.
12. Robertson KD. DNA methylation, methyltransferases, and cancer. Oncogene 2001;20:3139–55.
13. Balch C, Fang F, Matei DE, Huang TH, Nephew KP. Minireview: epigenetic changes in ovarian cancer. Endocrinology 2009;150:4003–11.
14. Jones PA, Issa JP, Baylin S. Targeting the cancer epigenome for therapy. Nat Rev Genet 2016;17:630–41.
15. Ghoshal K, Datta J, Majumder S, Bai S, Kutay H, Motiwala T, et al. 5-Aza-deoxycytidine induces selective degradation of DNA methyltransferase 1 by a proteasomal pathway that requires the KEN box, bromo-adjacent homology domain, and nuclear localization signal. Mol Cell Biol 2005; 25:4727–41.
16. Du Y, Yamaguchi H, Wei Y, Hsu JL, Wang HL, Hsu YH, et al. Blocking c-Met-mediated PARP1 phosphorylation enhances anti-tumor effects of PARP inhibitors. Nat Med 2016;22:194–201.
17. Fandy TE, Jiemjit A, Thakar M, Rhoden P, Suarez L, Gore SD. Decitabine induces delayed reactive oxygen species (ROS) accumulation in leukemia cells and induces the expression of ROS generating enzymes. Clin Cancer Res 2014;20:1249–58.
18. Matei D, Fang F, Shen C, Schilder J, Arnold A, Zeng Y, et al. Epigenetic resensitization to platinum in ovarian cancer. Cancer Res 2012;72: 2197–205.
19. Fu S, Hu W, Iyer R, Kavanagh JJ, Coleman RL, Levenback CF, et al. Phase 1b-2a study to reverse platinum resistance through use of a hypomethylating agent, azacitidine, in patients with platinum-resistant or platinum-refractory epithelial ovarian cancer. Cancer 2011; 117:1661–9.
20. Ha K, Lee GE, Palii SS, Brown KD, Takeda Y, Liu K, et al. Rapid and transient recruitment of DNMT1 to DNA double-strand breaks is mediated by its interaction with multiple components of the DNA damage response machinery. Hum Mol Genet 2011;20:126–40.

21. O'Hagan HM, Wang W, Sen S, Destefano Shields C, Lee SS, Zhang YW, et al. Oxidative damage targets complexes containing DNA methyltransferases, SIRT1, and polycomb members to promoter CpG Islands. Cancer Cell 2011;20:606–19.
22. Wang Y, Cardenas H, Fang F, Condello S, Taverna P, Segar M, et al. Epigenetic targeting of ovarian cancer stem cells. Cancer Res 2014;74: 4922–36.
23. Fang F, Cardenas H, Huang H, Jiang G, Perkins SM, Zhang C, et al. Genomic and epigenomic signatures in ovarian cancer associated with re-sensitization to platinum drugs. Cancer Res 2017;78:631–44.
24. Muvarak NE, Chowdhury K, Xia L, Robert C, Choi EY, Cai Y, et al. Enhancing the cytotoxic effects of PARP inhibitors with DNA demethylating agents - A potential therapy for cancer. Cancer Cell 2016;30:637–50.
25. Ozes AR, Miller DF, Ozes ON, Fang F, Liu Y, Matei D, et al. NF-kappaB-HOTAIR axis links DNA damage response, chemoresistance and cellular senescence in ovarian cancer. Oncogene 2016;35:5350–61.
26. Fan M, Yan PS, Hartman-Frey C, Chen L, Paik H, Oyer SL, et al. Diverse gene expression and DNA methylation profiles correlate with differential adaptation of breast cancer cells to the antiestrogens tamoxifen and fulvestrant. Cancer Res 2006;66:11954–66.
27. Chen D, Bhat-Nakshatri P, Goswami C, Badve S, Nakshatri H. ANTXR1, a stem cell-enriched functional biomarker, connects collagen signaling to cancer stem-like cells and metastasis in breast cancer. Cancer Res 2013; 73:5821–33.
28. Jensen RB, Carreira A, Kowalczykowski SC. Purified human BRCA2 stimulates RAD51-mediated recombination. Nature 2010;467:678–83.
29. Jensen RB, Ozes A, Kim T, Estep A, Kowalczykowski SC. BRCA2 is epistatic to the RAD51 paralogs in response to DNA damage. DNA Repair (Amst) 2013;12:306–11.
30. Chou TC, Talalay P. Quantitative analysis of dose-effect relationships: the combined effects of multiple drugs or enzyme inhibitors. Adv Enzyme Regul 1984;22:27–55.
31. Langdon SP, Lawrie SS, Hay FG, Hawkes MM, McDonald A, Hayward IP, et al. Characterization and properties of nine human ovarian adenocarcinoma cell lines. Cancer Res 1988;48:6166–72.
32. Sakai W, Swisher EM, Karlan BY, Agarwal MK, Higgins J, Friedman C, et al. Secondary mutations as a mechanism of cisplatin resistance in BRCA2-mutated cancers. Nature 2008;451:1116–20.
33. Murai J, Huang SY, Das BB, Renaud A, Zhang Y, Doroshow JH, et al. Trapping of PARP1 and PARP2 by clinical PARP inhibitors. Cancer Res 2012;72:5588–99.
34. Gelmon KA, Tischkowitz M, Mackay H, Swenerton K, Robidoux A, Tonkin K, et al. Olaparib in patients with recurrent high-grade serous or poorly differentiated ovarian carcinoma or triple-negative breast cancer: a phase 2, multicentre, open-label, non-randomised study. Lancet Oncol 2011;12: 852–61.
35. Kaufman B, Shapira-Frommer R, Schmutzler RK, Audeh MW, Friedlander M, Balmana J, et al. Olaparib monotherapy in patients with advanced cancer and a germline BRCA1/2 mutation. J Clin Oncol 2015;33:244–50.
36. Fang F, Munck J, Tang J, Taverna P, Wang Y, Miller DF, et al. The novel, small-molecule DNA methylation inhibitor SGI-110 as an ovarian cancer chemosensitizer. Clin Cancer Res 2014;20:6504–16.
37. El-Khamisy SF, Masutani M, Suzuki H, Caldecott KW. A requirement for PARP-1 for the assembly or stability of XRCC1 nuclear foci at sites of oxidative DNA damage. Nucleic Acids Res 2003;31:5526–33.
38. Trachootham D, Alexandre J, Huang P. Targeting cancer cells by ROS-mediated mechanisms: a radical therapeutic approach? Nat Rev Drug Discov 2009;8:579–91.
39. Villena J, Henriquez M, Torres V, Moraga F, Diaz-Elizondo J, Arredondo C, et al. Ceramide-induced formation of ROS and ATP depletion trigger necrosis in lymphoid cells. Free Radic Biol Med 2008;44:1146–60.
40. Martinez-Reyes I, Cuezva JM. The H(+)-ATP synthase: a gate to ROS-mediated cell death or cell survival. Biochim Biophys Acta 2014;1837: 1099–112.
41. Brunyanszki A, Olah G, Coletta C, Szczesny B, Szabo C. Regulation of mitochondrial poly(ADP-Ribose) polymerase activation by the beta-adrenoceptor/cAMP/protein kinase A axis during oxidative stress. Mol Pharmacol 2014;86:450–62.
42. Kim J, Wong PK. Oxidative stress is linked to ERK1/2-p16 signaling-mediated growth defect in ATM-deficient astrocytes. J Biol Chem 2009;284:14396–404.
43. Nishio K, Morikage T, Kubota N, Ohmori T, Takeda Y, Fujiwara Y, et al. Alteration of type II regulatory subunit of cAMP-dependent protein kinase in human cisplatin-resistant cells as a basis of collateral sensitivity to 8-chloro-cAMP. Jpn J Cancer Res 1992;83:754–60.
44. Ibrahim YH, Garcia-Garcia C, Serra V, He L, Torres-Lockhart K, Prat A, et al. PI3K inhibition impairs BRCA1/2 expression and sensitizes BRCA-proficient triple-negative breast cancer to PARP inhibition. Cancer Discov 2012;2:1036–47.
45. de Bono J, Ramanathan RK, Mina L, Chugh R, Glaspy J, Rafii S, et al. Phase I, dose-escalation, two-part trial of the PARP inhibitor talazoparib in patients with advanced germline BRCA1/2 mutations and selected sporadic cancers. Cancer Discov 2017;7:620–9.
46. Fang F, Balch C, Schilder J, Breen T, Zhang S, Shen C, et al. A phase 1 and pharmacodynamic study of decitabine in combination with carboplatin in patients with recurrent, platinum-resistant, epithelial ovarian cancer. Cancer 2010;116:4043–53.
47. Swindall AF, Stanley JA, Yang ES. PARP-1: Friend or foe of DNA damage and repair in tumorigenesis? Cancers (Basel) 2013;5:943–58.
48. Rohlff C, Safa B, Rahman A, Cho-Chung YS, Klecker RW, Glazer RI. Reversal of resistance to adriamycin by 8-chloro-cyclic AMP in adriamycin-resistant HL-60 leukemia cells is associated with reduction of type I cyclic AMP-dependent protein kinase and cyclic AMP response element-binding protein DNA-binding activities. Mol Pharmacol 1993;43:372–9.
49. Orta ML, Hoglund A, Calderon-Montano JM, Dominguez I, Burgos-Moron E, Visnes T, et al. The PARP inhibitor Olaparib disrupts base excision repair of 5-aza-2′-deoxycytidine lesions. Nucleic Acids Res 2014;42:9108–20.
50. Lord CJ, Ashworth A. PARP inhibitors: Synthetic lethality in the clinic. Science 2017;355:1152–8.